11th International Conference on Vibration Problems
Z. Dimitrovová *et al.* (eds.)
Lisbon, Portugal, 9-12 September 2013

NONLINEAR DYNAMIC CHARACTERISTICS AND CHAOS CONTROL OF GMF-SMA COMPOSITE BEAM IN AXIAL STOCHASTIC EXCITATION

Z. W. Zhu*[1], Q. X. Zhang[1], J. Xu [2]

[1] Department of Mechanics, Tianjin University
zhuzhiwentju@163.com, zqxfirst@163.com

[2] Tianjin Key Laboratory of Nonlinear Dynamics and Chaos Control
xujia_ld@163.com

Keywords: Piezoelectric Ceramics, Shape Memory Alloy, Composite Beam, Stochastic Hopf Bifurcation, Chaos Control.

Abstract. *Nonlinear dynamic characteristics and chaos control of giant magnetostrictive film (GMF)-shape memory alloy (SMA) composite simply-supported beam subjected to axial stochastic excitation were studied in this paper. Giant magnetostrictive film was prepared based on SMA beam to be GMF-SMA composite beam. Von de Pol item was introduced to interpret the hysteretic phenomena of both giant magnetostrictive material and SMA, and the nonlinear dynamic model of GMF-SMA composite beam subjected to axial stochastic excitation was developed. The stochastic stability and stochastic Hopf bifurcation of the system was analyzed, and the steady-state probability density function of the dynamic response of the system were obtained. The conditions of stochastic chaos were solved in stochastic Melnikov method, and the boundary of safe basin of the system was obtained. Finally, the stochastic optimal control strategy which aimed to the maximization of reliability was obtained in stochastic dynamic programming method. The reliability function of the system was solved, and then the probability density of the first-passage time was obtained. Numerical simulation shows that the stability of the trivial solution varies with bifurcation parameter, and stochastic Hopf bifurcation appears in the process; the boundary of safe basin of the system has fractal characteristics, which means chaos induced by noise; the reliability of the system is improved by stochastic optimal control, the boundary of safe basin is extended and the first-passage time is delayed. GMF-SMA composite beam combines the advantages of both GMF and SMA, and can reduce vibration through passive control and active control effectively. The results of this paper are helpful to application of GMF-SMA composite beam in engineering fields.*

1 INTRODUCTION

Shape Memory Alloy (SMA) is a kind of smart material and applied in engineering field widely. It has many special characteristics such as shape memory, large damping and superelasticity, based on which the SMA smart structure can be designed to reduce vibration. Although SMA has excellent characteristics for vibration reduction, the long response time limits its its application. For improving response of SMA smart structure, giant magnetostrictive film (GMF) was prepared based on SMA beam, which was known as GMF-SMA composite beam. GMF has many special characteristics such as giant strain, rapid response, and excellent control precision, which can control structure vibration effectively. GMF-SMA composite beam combines the advantages of both GMF and SMA, and can reduce vibration in both passive control and active control effectively.

Many scholars studied SMA beam and GMF respectively [1-8]. Lau analyzed vibration characteristics of SMA beams with different boundary conditions [1]. Liew studied the pseudoelastic behavior of a SMA beam by the element-free Galerkin method [2]. Zbiciak discussed dynamic characteristics of pseudoelastic SMA beam [3]. Scarpa developed spectral element formulation for SMA beams under random vibration excitation [4]. In GMF field, Jia developed nonlinear magnetomechanical coupling model of GMF at low magnetic fields [5]. Yang proposed a kind of dynamic model of magnetic system constructed with GMF using element-free Galerkin method [6]. Masuda created high responsiveness composite mover device constructed with positive and negative GMF [7]. Tiercelin used GMF to achieve nonlinear actuation of cantilevers, and studied response of the system in sub-harmonic excitation [8]. Although many achievements in the dynamic characteristics of GMF and SMA were obtained in the past years, the theoretical results of GMF-SMA composite beam were not abundant because of the complex nonlinear characteristics of GMF and SMA.

This paper aims to offer a kind of analysis method to nonlinear dynamical characteristics of GMF-SMA composite beam in axial stochastic excitation. Von del Pol item was improved to interpret the hysteretic loop of SMA and GMF. The nonlinear dynamic model of GMF-SMA composite simply supported beam subjected to axial stochastic excitation was developed, and the stochastic bifurcation characteristics of the system were analyzed. Finally, the stochastic optimal control strategy was proposed to improve the reliability of the system.

2 HYSTERESIS NONLINEAR MODEL OF GMF-SMA COMPOSITE BEAM SUBJECTED TO AXIAL STOCHASTIC EXCITATION

The structure of GMF-SMA composite beam was shown in Figure 1. It was made up of giant magnetostrictive film (GMF) and SMA beam. The structure can be simplified as single SMA beam since the thickness of SMA was 150 μm and that of GMF was only 10-100 nm.

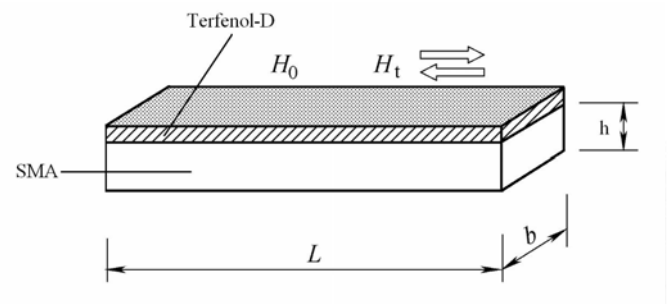

Figure 1: Structure of GMF-SMA composite beam.

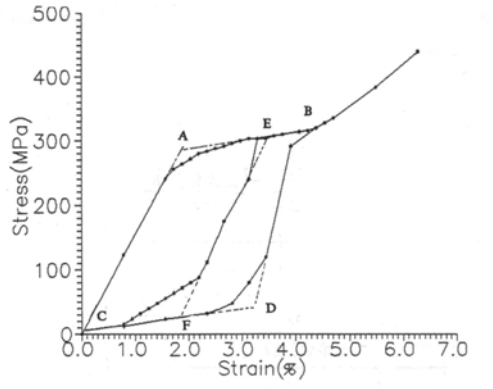

Figure 2: Strain-stress curves of SMA.

The strain-stress curves of SMA were shown in Figure 2. Obviously, there are hysteretic phenomena in SMA. Most of SMA models were based on thermodynamics theory and micromechanics theory, where the percentage content of martensite was taken as main variable of stress-strain equation. As results, those SMA models were mostly shown as equations with subsection function or double integral function, and hard to be analyzed in theory [9-11]. Usually, research results to those models can only be obtained by numerical method or experiment method. In this paper, improved Von del Pol hysteretic model was introduced to describe the hysteretic nonlinear characteristics of the strain-stress curves of SMA as follows:.

$$\sigma = f_1(\varepsilon) + f_2(\varepsilon) = a_1\varepsilon + a_2\varepsilon^2 + a_3\varepsilon^3 + (a_4\varepsilon + a_5\varepsilon^2 + a_6\varepsilon^3 + a_7\varepsilon^4)\dot{\varepsilon} \tag{1}$$

where σ is stress, ε is strain, a_i (i=1~7) are coefficients, $f_1(x) = \sum_{i=1}^{3} a_i x^i$ is skeleton curve of hysteretic loop; $f_2(x) = (a_4\varepsilon + a_5\varepsilon^2 + a_6\varepsilon^3 + a_7\varepsilon^4)\dot{\varepsilon}$ is improved Von del Pol item, which describes is the difference between the skeleton curve and the hysteretic loop;

Partial least-square regression method was used to test the fitting effect of Eq. (1). The result of principal component analysis based on experimental data was shown in Figure 3, and the values of the coefficients were shown in Figure 4. We can see that all of the items are remarkable.

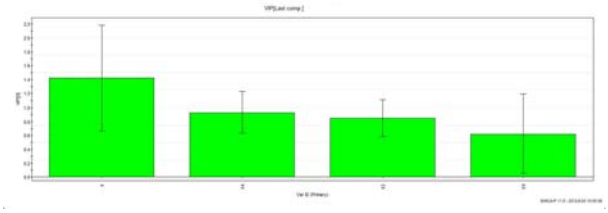

Figure 3: Analysis result of principal component.

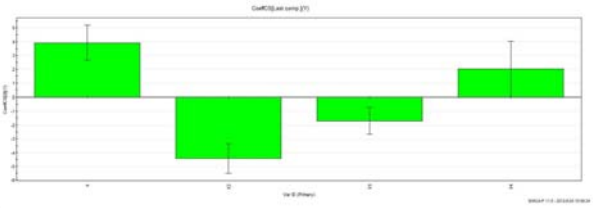

Figure 4: Values of the coefficients.

The result of forecast test to Eq. (1) was shown in Figure 5, where red line is real data and black line is forecast value. We can see that Eq. (1) can describe the real curve well.

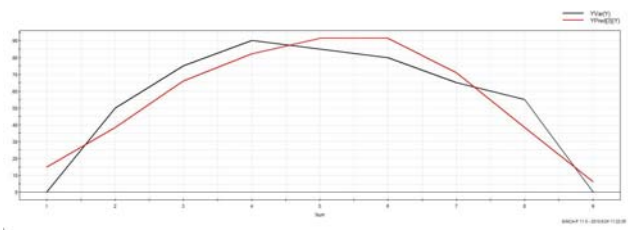

Figure 5: Results of forecast test.

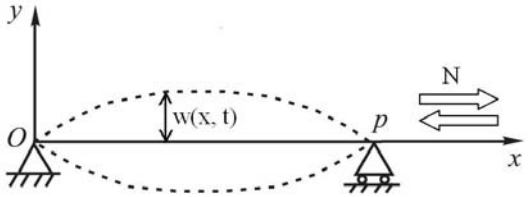

Figure 6: Mechanical model of GMF-SMA composite beam.

The mechanical model of GMF-SMA composite simply-supported beam subjected to axial stochastic excitation was shown in Figure 6, where $w(x,t)$ is the mode of SMA beam, N is axial excitation, $N = F_0 - F\xi(t)$, F_0 is initial excitation, F is coefficient, $\xi(t)$ is Gauss white noise whose mean is zero and intensity is 2D, D>0. Thus, the dynamical equation of GMF-SMA simply supported beam subjected to axial stochastic excitation can be shown as follows:

$$\frac{\partial^2 M}{\partial x^2} + N\frac{\partial^2 w}{\partial x^2} + c\frac{\partial w}{\partial t} + \rho A\frac{\partial^2 w}{\partial t^2} = 0 \tag{2}$$

where c is linear damping coefficient, ρ is density of the SMA, and A is area of the cross-section of SMA beam, M is the bending moment,

$$M = \int -\sigma y dA = b\int_{-h/2}^{h/2} -y[a_1\varepsilon + a_2\varepsilon^2 + a_3\varepsilon^3 + (a_4\varepsilon + a_5\varepsilon^2 + a_6\varepsilon^3 + a_7\varepsilon^4)\dot{\varepsilon}]dy \tag{3}$$

Since $w(t,x)=u(t)\sin(\frac{\pi}{l}x)$ and $\varepsilon=-y\frac{\partial^2 w}{\partial x^2}$, we obtained:

$$M=-I_1a_1\pi^2u\sin(\frac{\pi}{l}x)-I_3a_3\pi^6u^3\sin^3(\frac{\pi}{l}x)-I_3a_5\pi^6u^2\sin^3(\frac{\pi}{l}x)\dot{u}-I_5a_7\pi^{10}u^4\sin^5(\frac{\pi}{l}x)\dot{u} \tag{4}$$

where $u(t)$ is amplitude of the fundamental mode, $I_1=\frac{bh^3}{12l^2}$, $I_3=\frac{bh^5}{80l^6}$, $I_5=\frac{bh^7}{448l^{10}}$. Thus, the differential equation of vibration amplitude with parametric excitation can be solved from Eq. (2) as follows:

$$\ddot{u}+\frac{a_1I_1\pi^4-F_0\pi^2}{\rho Al^2}u+(\frac{c}{\rho A}+\frac{3a_5I_3\pi^8}{4\rho Al^2}u^2+\frac{5a_7I_5\pi^{12}}{8\rho Al^2}u^4)\dot{u}+\frac{3a_3I_3\pi^8}{4\rho Al^2}u^3=\frac{F\pi^2}{\rho Al^2}u\xi(t) \tag{5}$$

3 STOCHASTIC BIFURCATION AND STOCHASTIC CHAOS OF THE SYSTEM

3.1 Stochastic Bifurcation

Let $u=q$, $\dot{u}=p$, Eq. (5) can also be shown as follows:

$$\begin{cases}\dot{q}=p\\ \dot{p}=-\mathrm{b}_1q-\mathrm{b}_3q^3-(2\eta+b_5q^2+b_7q^4)p+eq\varsigma(t)\end{cases} \tag{6}$$

The Hamiltonian function of Eq. (6) can be shown as follows:

$$H=\frac{1}{2}p^2+\frac{1}{2}b_1q^2+\frac{1}{4}b_3q^4 \tag{7}$$

According to the quasi-nonintegrable Hamiltonian system theory, the Hamiltonian function H(t) converges weakly in probability to an one-dimensional Ito diffusion process shown as follows:

$$dH=m(H)dt+\sigma(H)dB(t) \tag{8}$$

where $B(t)$ is standard Wiener process, $m(H)$ and $\sigma(H)$ are drift and diffusion coefficients of Ito stochastic process, which can be obtained in stochastic averaging method:

$$m(H)=(\frac{De^2}{b_1}-2\eta)H-\frac{b_5}{2b_1}H^2-\frac{b_7}{2b_1^2}H^3 \tag{9}$$

$$\sigma^2(H)=\frac{De^2}{b_1}H^2 \tag{10}$$

The averaged FPK equation of Eq. (8) is:

$$\frac{\partial f}{\partial t}=-\frac{\partial}{\partial H}[m(H)f]+\frac{1}{2}\frac{\partial^2[\sigma^2(H)f]}{\partial H^2} \tag{11}$$

where f is probability density.

Thus, the stationary probability density function of the system is:

$$f(H)=\overline{A}\exp(-\int_0^H\left\{[\frac{d\sigma^2}{dt}-2m(t)]/\sigma^2\right\}dt)=\overline{A}H^{-\frac{4\eta b_1}{De^2}}\exp[-\frac{b_5}{De^2}H-\frac{b_7}{2De^2b_1}H^2] \tag{12}$$

where $\overline{A}$ is a normalization constant, $H=\frac{1}{2}p^2+\frac{1}{2}b_1q^2$.

From Eq. (12), we can see that:

1） η is linear damping coefficient, $\eta\geq 0$;

2） To $\eta = 0$, $H^{-\frac{4\eta b_1}{De^2}} = 1$, and the stationary probability density $f(H)$ is determined by the item $\exp[-\frac{b_5}{De^2}H - \frac{b_7}{2De^2 b_1}H^2]$. Especially, if $b_5 < 0$ and $b_7 > 0$, the stationary probability density will increases firstly, then decreases when H increases. It means that a limit loop will appear in the stationary probability density.

3） To $\eta > 0$, $H^{-\frac{4\eta b_1}{De^2}}$ decreases when H increases. To linear damping system, especially, the nonlinear damping coefficients b_5 and b_7 are both zero. It means that the stationary probability density $f(H)$ is determined only by the item $H^{-\frac{4\eta b_1}{De^2}}$, and will decreases when H increases. Thus, the origin (0,0) , which means the trivial solution H=0, should have the highest probability density;

4） In general, the steady-state probability density $f(H)$ is determined by η, b_5 and b_7. When H is very little, the item $H^{-\frac{4\eta b_1}{De^2}}$ will be remarkable; when H increases, the item $\exp[-\frac{b_5}{De^2}H]$ will be remarkable; when H is large enough, the item $\exp[-\frac{b_7}{2De^2 b_1}H^2]$ will be remarkable. In this process, the stationary probability density $f(H)$ will decreases firstly, then increases, and finally decreases when H increases;

5） Stochastic Hopf bifurcation appears in the varying process of the bifurcation parameters η, b_5 and b_7.

The results of numerical simulation of piezoelectric energy harvester were shown in Figure 7, where $b_1 = 100$, $D = 0.5$, $b_3 = 150$, $l = 1$, $M = 40$, $E = 2\times10^{11}$, $A = 8\times10^{-4}$, $I = 6\times10^{-11}$.

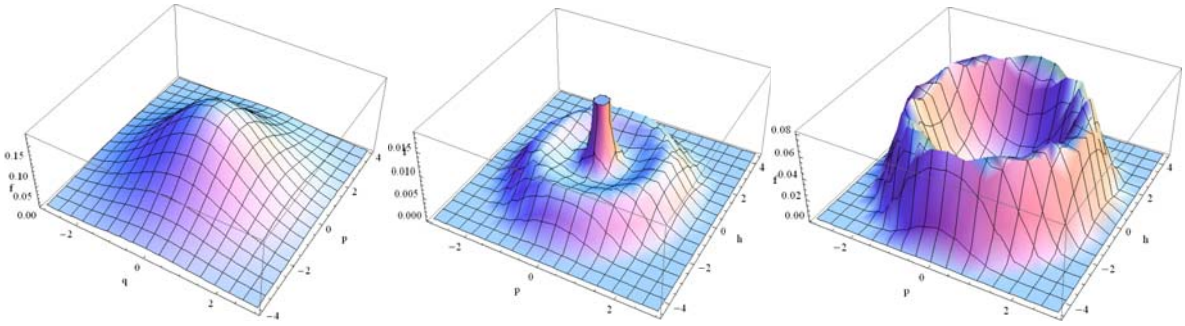

(a) η=0.3, b_5 =0, b_7 =0 (b) η=0.2, b_5 =-3.5, b_7 =1 (c) η=0, b_5 =-3.5, b_7 =1

Figure7: Stationary probability density of the system.

From Figure 7, we can see that:

6） p=0 and q=0 when H =0, so the trivial solution H =0 corresponds to the origin (0, 0) in the probability density;

7） The steady-state probability density of H=0 is the max when η=0.3, b_5 =0, b_7 =0;

8） The steady-state probability density varies when H increases, and stochastic Hopf bifurcation appears in the varying process of the bifurcation parameters η, b_5 and b_7. We can obviously see that there is a limit cycle in the figures of probability den-

sity, which is caused by hysteretic nonlinear damping coefficients b_5 and b_7. The results of simulation were accord with the analysis ones.

3.2 Stochastic chaos

The equations for homoclinical orbits of Eq. (6) can be shown as follows:

$$q(t) = \pm\sqrt{-2b_1}\,\mathrm{sec}\,h(\sqrt{-b_1}t) \tag{13}$$

$$p(t) = \mp\sqrt{2b_3}b_1\,\mathrm{sec}\,h(\sqrt{-b_1}t)\tan c(\sqrt{-b_1}t) \tag{14}$$

The stochastic Melnikov integration is

$$M(t_1) = \int_{-\infty}^{+\infty} p[-(2\eta + b_5q^2 + b_7q^4)p + eq\varsigma(t_1 - t)]dt = -I + z(t_1) \tag{15}$$

where $z(t_1) = \int_{-\infty}^{+\infty} epq\varsigma(t_1 - t)dt$. The item $-I$ represents the mean of the Melnikov process due to damping force, and $z(t_1)$ denotes the random portion of the Melnikov process due to the bounded noise $\varsigma(t)$. Thus, the variance of $z(t_1)$ as the output of the system can be expressed as follows:

$$\sigma_z^2 = \int_{-\infty}^{+\infty} |H(\omega)^2| S(\omega)d\omega \tag{16}$$

where $S(\omega)$ is the spectral density of $\varsigma(t)$, and $H(\omega)$ is the frequency response function of the system, $H(\omega) = eq\int_{-\infty}^{+\infty} p(t)e^{-i\omega t}dt$.

The criterion for chaotic motion based on Melnikov process is:

$$[-\frac{8\eta}{3b_3}b_1^{\frac{3}{2}} - \frac{16b_5}{15b_3^2}b_1^{\frac{5}{2}}]^2 \le \frac{D}{2\pi}\int_{-\infty}^{+\infty} H^2(\omega)d\omega \tag{17}$$

The system parameters were chosen as: $b_1 = -1$, $b_3 = 4$, $\eta = 0.38$, $b_5 = -0.22$, $b_7 = 0.02$, $D = 1$, then We obtained:

$$0.057 \le 0.053e^2$$

The reliability function $R(H,t)$ of the system was determined as follows:

$$\sup\left\{[m(H) + \frac{1}{2}\sigma^2(H)\frac{\partial^2 R}{\partial H^2}\right\} = -1 \tag{18}$$

The boundary of safe basin of the system can be determined by Eq. (18) when the required reliability was given. Obviously, we can see that the Hamiltonian value *H* of the system is related to the reliability.

Some points in safe basin, however, will finally leave the safe basin in chaotic motion due to stochastic excitation, which cause the boundary of safe basin become fractal. The fractal phenomenon of the boundary of safe basin was called basin erosion. To obtain the fractal boundary, we firstly determine the boundary of safe basin of the system without stochastic excitation shown as follows:

$$G = \left\{(p,q)\left|\frac{1}{2}p^2 + \frac{1}{2}b_1q^2 + \frac{1}{4}b_3q^4 < H\right.\right\} \tag{19}$$

Then we computed the trajectory of every phase points in safe basin according to Eq. (6). The motion of the phase point was defined as unsafe when the Hamiltonian value of the phase point is larger than the given value *H*, and then the phase point was considered as leaving the safe basin and deleted. The variation of safe basin subjected to white noise excitation was shown in Figure 8.

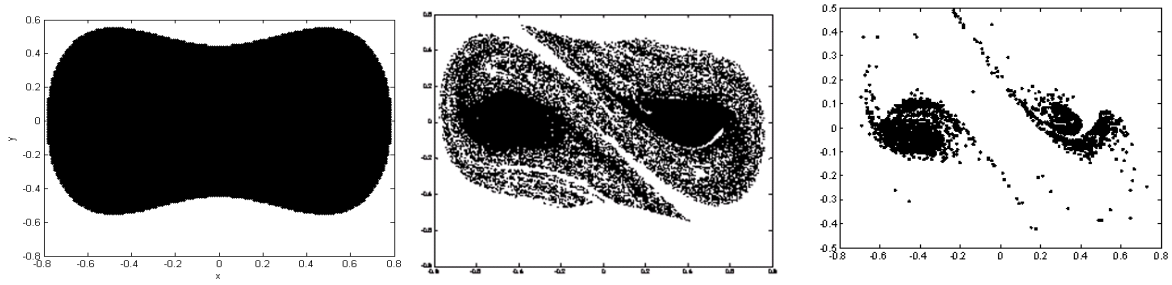

(a) e =0 (b) e =1 (c) e =3

Figure8: Safe basin subjected to stochastic excitation.

From Figure 8, we can see that the area of safe basin decreases when the Gaussian white noise excitation increases, and the boundary of safe basin becomes fractal, which means chaos induced by noise.

4 STOCHASTIC OPTIMAL CONTROL OF SYSTEM RELIABILITY

From Chapter 3, we can see that stochastic Hopf bifurcation appears in the varying process of the bifurcation parameters η, b_5 and b_7. Stochastic Hopf bifurcation changes the motion of the system, and causes the reliability of the system decreases. In this chapter, stochastic optimal control was introduced to improve the reliability of the system.

The dynamic model of controlled system can be shown as follows:

$$\begin{cases} \dot{q} = p \\ \dot{p} = -\mathrm{b}_1 q - \mathrm{b}_3 q^3 - (2\eta + b_5 q^2 + b_7 q^4)\, p + eq\varsigma(t) + F(t) \end{cases} \tag{20}$$

where $F(t)$ is active control force. To GMF-SMA composite beam, the active control force was supplied by GMF drived by magnetic field.

The strain- magnetic field intensity (MFI) curves of GMF were shown in Figure 9. Obviously, there are hysteretic loop in GMF. Similar to SMA, the strain- MFI curves of GMF can be expressed as follows:

$$H_M = c_1\varepsilon + c_2\varepsilon^2 + c_3\varepsilon^3 + (c_4\varepsilon + c_5\varepsilon^2 + c_6\varepsilon^3 + c_7\varepsilon^4)\dot{\varepsilon} \tag{21}$$

where $c_i (i = 1 \sim 7)$ are coefficients and can be determined by partial least-square regression method.

According to the quasi Hamiltonian theory, the one-dimensional Ito diffusion process of Eq. (20) can be shown as:

$$dH = [m(H) + \frac{1}{T(H)} \int_\Gamma F(t) dq] dt + \sigma(H) dB(t) \tag{22}$$

where $T(H) = \int_\Gamma \frac{1}{p} dq$, $\Gamma = \left\{ q \middle| \frac{1}{2} kq^2 \le H \right\}$.

The reliability function $R(H,t)$ of the system was determined by the dynamic programming principle shown as follows:

$$\sup\left\{ [m(H) + \frac{1}{T(H)} \int_\Gamma F(t) dq] \frac{\partial R}{\partial H} + \frac{1}{2} \sigma^2(H) \frac{\partial^2 R}{\partial H^2} \right\} = -1 \tag{23}$$

The optimal control force F^* should make the reliability function the maximum, so it can be designed as follows:

$$F^* = b \,\mathrm{sign}\left(\frac{\partial H}{\partial p} \frac{\partial R}{\partial H}\right) \tag{24}$$

where b is the intense of control force. For $\frac{\partial R}{\partial H} < 0$, Eq. (24) can be simplified as follows:

$$F^* = -b\,\mathrm{sign}(\frac{\partial H}{\partial p}) \tag{25}$$

$\varepsilon = \frac{\sigma}{E} = \frac{F(t)}{E\overline{A}}$ can be determined when the control force $F(t)$ was designed, where σ is stress, E is modulus of elasticity, $\overline{A}$ is area of the cross-section of GMF. Thus, the intensity of control magnetic field H_M can be determined according to Eq. (21).

Substituting Eq. (25) into Eq. (22), we obtained

$$dH = [m(H) - \frac{2\sqrt{2}b}{\pi} H^{\frac{1}{2}}]dt + \sigma(H)dB(t) \tag{26}$$

Thus, the background Kolmogorov equation (BK equation) can be shown as follows:

$$\frac{\partial R}{\partial t} = [m(H) - \frac{2\sqrt{2}b}{\pi} H^{\frac{1}{2}}]\frac{\partial R}{\partial H} + \frac{1}{2}\sigma^2(H)\frac{\partial^2 R}{\partial H^2} \tag{27}$$

The initial condition is:

$$R(H_0,0) = 1,\ H_0 \in \Gamma \qquad \text{when } t = 0 \tag{28}$$

The boundary conditions are:

$$R(H_0,t) = 0 \qquad \text{when } H_0 = \Gamma$$

$$\frac{\partial R}{\partial t} = [m(H) - \frac{2\sqrt{2}b}{\pi} H^{\frac{1}{2}}]\frac{\partial R}{\partial H} \qquad \text{when } H_0 = 0$$

The probability density $p(H_0,t)$ of first-passage time (FPT) of the controlled system was determined as follows:

$$p(H_0,T) = -\left.\frac{\partial R}{\partial t}\right|_{t=T} \tag{29}$$

The result of numerical simulation of reliability function and probability density of first-passage time of the controlled system were shown in Figure10 and Figure11, where D=1, H=3, b=0/1/3.

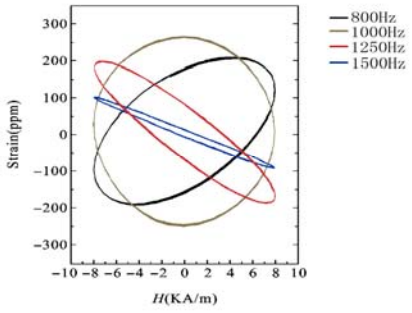

Figure 9: Strain- MFI curves of GMF.

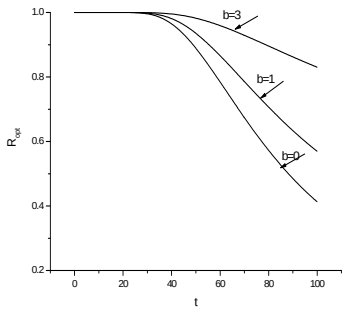

Figure 10: Reliability of system.

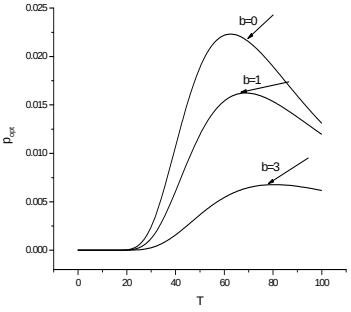

Figure 11: Probability density of first-passage time.

From Figure 10 and Figure 11, we can see that:

1) The reliability function $R(H,t)$ decreases when time increases;
2) The reliability of the system was improved obviously when the control force increases, which means that the control strategy was effective;
3) The probability density of first-passage time increases with time. First-passage means the system leaves the safe area, which will cause the system unstable.
4) First-passage time can be delayed by the control force, which also means that the control force can enhance the reliability of the system.

The variation of safe basin of the system subjected to white noise excitation and active control force was shown in Figure 12. We can see that the area of safe basin increases when the control force increases, and the boundary of safe basin becomes smooth. It means that the control force can eliminate fractal boundary and chaotic motion

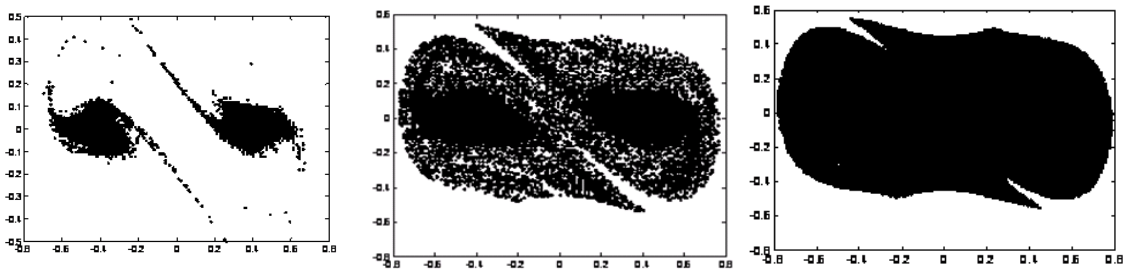

(a) b =0 (b) b =1 (c) b =3

Figure 12: Safe basin subjected to stochastic excitation and control force.

5 CONCLUSIONS

In this paper, nonlinear dynamic characteristics and chaos control of giant magnetostrictive film (GMF)-shape memory alloy (SMA) composite simply-supported beam subjected to axial stochastic excitation were studied. Giant magnetostrictive film was prepared based on SMA beam to be GMF-SMA composite beam. Von de Pol item was improved to interpret the hysteretic phenomena of both giant magnetostrictive material and SMA, and the nonlinear dynamic model of GMF-SMA composite beam subjected to axial stochastic excitation was developed. The stochastic Hopf bifurcation of the system was analyzed, and the steady-state probability density function of the dynamic response of the system was obtained. The conditions of stochastic chaos were solved in stochastic Melnikov method, and the boundary of safe basin of the system was obtained. Finally, the stochastic optimal control strategy which aimed to the maximization of reliability was proposed. The reliability function of the system was solved, and the probability density of the first-passage time was obtained. Numerical simulation shows that the stability of the trivial solution varies with bifurcation parameters, and stochastic Hopf bifurcation appears in the process; the boundary of safe basin of the system has fractal characteristics, which means chaos induced by noise; the reliability of the system is improved by stochastic optimal control, the boundary of safe basin is extended and the first-passage time is delayed. GMF-SMA composite beam combines the advantages of both GMF and SMA, and can reduce vibration through passive control and active control effectively. The results of this paper are helpful to application of GMF-SMA composite beam in engineering fields.

ACKNOWLEDGMENT

The authors gratefully acknowledge the support of Natural Science Foundation of China (NSFC) through grant no. 11272229, the Ph.D. Programs Foundation of Ministry of Education of China through grant no. 20120032120006, and Tianjin Research Program of Application Foundation and Advanced Technology through grant no. 13JCYBJC17900.

REFERENCES

[1] K. T. Lau, Vibration characteristics of SMA composite beams with different boundary conditions. *Materials and Design*, **23**, 741–749, 2002.

[2] K. M. Liew, J. Ren, S. Kitipornchai, Analysis of the pseudoelastic behavior of a SMA beam by the element-free Galerkin method. *Engineering Analysis with Boundary Elements*, **28**, 497–507, 2004.

[3] A. Zbiciak, Dynamic analysis of pseudoelastic SMA beam. *International Journal of Mechanical Sciences*, **52**, 56–64, 2010.

[4] F. Scarpa, M. Ruzzene, M. R. Hassan, Spectral element formulation for SMA beams under random vibration excitation. *Smart Structures and Materials*, **33**, 286–293, 2004.

[5] Z. Y. Jia, W. Liu, Y. S. Zhang, A nonlinear magnetomechanical coupling model of giant magnetostrictive thin films at low magnetic fields. *Sensors and Actuators A-Physical*, **128**, 158–164, 2006.

[6] Q. X. Yang, H. Y. Chen, S. Z. Liu, Dynamic modeling of a magnetic system constructed with giant magnetostrictive thin film using element-free Galerkin method. *IEEE Transactions on Magnetics*, **42**, 939–942, 2006.

[7] S. Masuda, Y. Matsumura, Y. Nishi, High responsiveness composite mover device constructed with positive and negative giant magnetostrictive films. *Journal of Japan Institute of Metals*, **70**, 166–168, 2006.

[8] N. Tiercelin, V. Preobrazhensky, P. Pernod, Sub-harmonic excitation of a planar magneto-mechanical system by means of giant magnetostrictive thin films. *Journal of Magnetism and Magnetic Materials*, **210**, 302–308, 2000.

[9] K. Tanaka, A thermomechanical sketch of shape memory effect: one-dimensional tensile behavior. *Res Mechanics*, **18**, 251–263, 1986.

[10] J. G. Boyd, D. C. Lagoudas, Thermodynamical constitutive model for shape memory materials. *International Journal of P1asticity*, **12**, 805–842, 1996.

[11] L. C. Brinson, One-dimensional constitutive behavior of shape memory alloys: thermomechanical derivation with nonconstant material functions and redefined martensite internal variable. *Journal of Intelligent Material Systems and Structures*, **4**, 229–242, 1993.